- 1 Mapping peatland heterogeneity: A key to assessing carbon balance and its
- 2 radiative effect within a northern boreal landscape
- 3 Running Title: Boreal peatland heterogeneity and carbon balance

4

- 5 Dan Kou^{1,2*}, Tarmo Virtanen³, Claire C. Treat⁴, Juha-Pekka Tuovinen⁵, Aleksi
- 6 Räsänen^{3,6}, Sari Juutinen³, Juha Mikola^{3,7}, Mika Aurela⁵, Lauri Heiskanen⁵, Maija
- 7 Heikkilä³, Jan Weckström³, Teemu Juselius³, Sanna R. Piilo³, Jia Deng⁸, Yu Zhang⁹,
- 8 Nitin Chaudhary^{10,11}, Conghong Huang¹², Minna Väliranta³, Christina Biasi¹,
- 9 Mingyang Guo², Qianlai Zhuang², Atte Korhola³, and Narasinha J. Shurpali¹³

- ¹Biogeochemistry Research Group, Department of Biological and Environmental
- 12 Sciences, University of Eastern Finland, Kuopio, Finland.
- ²Department of Earth, Atmospheric, and Planetary Sciences, Purdue University, West
- 14 Lafayette, Indiana, USA.
- 15 ³Ecosystems and Environment Research Programme, Faculty of Biological and
- 16 Environmental Sciences, and Helsinki Institute of Sustainability Science (HELSUS),
- 17 University of Helsinki, Helsinki, Finland.
- ⁴Permafrost Research Section, Alfred Wegener Institute Helmholtz Centre for Polar
- and Marine Research, Potsdam, Germany.
- ⁵Finnish Meteorological Institute, Helsinki, Finland.
- 21 ⁶Natural Resources Institute Finland (Luke), Oulu, Finland.
- ⁷Carbon cycle management, Department of Bioeconomy and Environment, Natural
- 23 Resources Institute Finland, Helsinki, Finland.

24	⁸ Earth Systems Research Centre, Institute for the Study of Earth, Oceans and Space,
25	University of New Hampshire, Durham, New Hampshire, USA.
26	⁹ Canada Centre for Remote Sensing, Natural Resources Canada, Ottawa, Canada.
27	¹⁰ Department of Geosciences, University of Oslo, Oslo, Norway.
28	¹¹ Department of Physical Geography and Ecosystem Science, Lund University, Lund,
29	Sweden.
30	¹² Department of Epidemiology and Environmental Health, University at Buffalo,
31	Buffalo, New York, USA.
32	¹³ Production Systems, Natural Resources Institute Finland, Maaninka, Finland.
33	
34	*Correspondence: Dr. Dan Kou, E-mail: dan.kou@uef.fi; dan.kou1120@gmail.com
35	Manuscript type: Primary Research Article
36	
37	Manuscript submitted to Global Change Biology
38	29th-August-2021
39	Manuscript information: 53 pages, 6 figures, 3 tables, 1 supplementary text, 7
40	supplementary tables, 17 supplementary figures

Abstract

41

42

43

44

45

46

47

48

49

50

51

52

53

54

55

56

57

58

59

Boreal peatlands are highly heterogeneous and play a significant role in the global carbon (C) cycle. However, the effects of the peatland-dominated heterogeneity within the boreal landscape are rarely quantified. Here, we use field-based measurements, high-resolution land cover classification, and biogeochemical and atmospheric models to estimate the C budget and corresponding radiative effect (RE) for a boreal landscape (Kaamanen) that is rich in peatlands and aquatic ecosystems. The average present-day, landscape-scale CO₂ and CH₄ budgets were -108 \pm 10 and 2.28 \pm 0.19 g C m⁻² yr⁻¹, respectively. We find that peatland heterogeneity accounts for 88% of the variability in CH₄-C budget across the Kaamanen landscape despite only comprising 26% of the area. Moreover, peatland heterogeneity dominates the variability in RE that combines CO₂ and CH₄ exchanges within the landscape, accounting for 65% and 79% over the 100-yr and 25-yr time horizons, respectively. Future warming tends to enhance this heterogeneity. Aggregating peatland classification or mis-classifying peatlands can significantly alter the estimated magnitude and even the sign of the RE due to landscape-scale C exchanges. Scrutiny of global land cover products revealed significant shortcomings in their representation of boreal peatlands, calling for improved mapping of boreal peatland heterogeneity to reduce the uncertainty in C budgets and C-climate feedback.

60

61

Keywords: boreal, landscape, peatland, heterogeneity, carbon, radiative effect

1 Introduction

The boreal biome, consisting of forest, peatland, and lake ecosystems, occurs in continental interiors at 45.5-71.4°N and covers about 15.1 million km² or 10.3% of Earth's land surface area (Helbig et al., 2020; Olson et al., 2001). This vast and patterned area stores more carbon (C) than the atmosphere (~ 1000 GtC vs. 860 GtC), most of which resides in soils and peatlands (Bradshaw & Warkentin, 2015; Friedlingstein et al., 2020; Hugelius et al., 2020; Nichols & Peteet, 2019). Moreover, the boreal ecosystems are vulnerable to environmental changes (Åberg, Jansson, & Jonsson, 2010; Hopple et al., 2020; Loisel et al., 2021), and thus their functioning in the changing climate is vital to the global C budget (Comyn-Platt et al., 2018; Gauthier, Bernier, Kuuluvainen, Shvidenko, & Schepaschenko, 2015; Tagesson et al., 2020).

Landscape processes are important for the upscaling of C budget across a biome since Earth System Models (ESMs) or statistical models such as machine learning are generally performed based on grid cells that are composed of multiple land units (Lawrence et al., 2018). A typical boreal landscape shows a mosaic of diverse forests, peatlands, and water bodies with large differences in their abiotic and biotic characteristics (Chapin III, Matson, & Vitousek, 2011; Hugelius et al., 2020; Verpoorter, Kutser, Seekell, & Tranvik, 2014). Therefore, the exploration of C budget and its climate impact at the landscape scale by considering the mosaic structure is crucial for accurately estimating the C budget across the boreal biome and hence for better understanding global C-climate feedbacks.

Despite their significance, our understanding of the landscape-scale C dynamics, including both carbon dioxide (CO₂) and methane (CH₄), in the circumpolar region mainly derives from tundra (Sturtevant & Oechel, 2013; Treat et al., 2018; Weller et al., 1995) and the transition zone between the tundra and boreal biomes (Christensen et al., 2007; O'Shea et al., 2014; Tang et al., 2015). Within the boreal biome, most studies have been aimed at the C dynamics of individual ecosystems (Clemmensen et al., 2013; Guo et al., 2020; Johansson et al., 2006) or the entire boreal zone (Kicklighter, Melillo, Monier, Sokolov, & Zhuang, 2019; Tagesson et al., 2020), with only a few landscapescale studies that consider both CO₂ and CH₄ exchange and forest, peatland, and aquatic ecosystems at the same time. These studies have advanced our understanding for example by showing the difference between short- and long-term C dynamics within a catchment (Juutinen et al., 2013), the need for integrating terrestrial and aquatic fluxes at the landscape scale (Aurela et al., 2015; Chi et al., 2020; Juutinen et al., 2013), and the application of airborne measurements of CO₂ and CH₄ fluxes to regional upscaling (O'Shea et al., 2014). In spite of these advances, there are major knowledge gaps. First, a fine-resolution mapping of different land cover types (LCTs) within a peatland complex, and thus the detailed quantification of heterogeneity in peatland C dynamics relative to the landscape-scale heterogeneity, is lacking. Second, remote sensing-based land cover classification is prone to classification errors. For example, peatlands adjacent to or embedded in forests may become classified as forests (Thompson, Simpson, & Beaudoin, 2016), and peatlands adjacent to lakes and flooded areas classified as lakes (Matthews, Johnson, Genovese, Du, & Bastviken, 2020). Little is known about how such LCT aggregation or misclassification affects the estimated landscape-scale C budgets. Third, our knowledge of the potential trajectories of the LCT-specific C budget heterogeneity under future warming conditions is limited. These

85

86

87

88

89

90

91

92

93

94

95

96

97

98

99

100

101

102

103

104

105

106

107

108

knowledge gaps undermine current C inventories, remote sensing-based upscaling products and procedures, and especially ESMs, in which the peatlands are considered as a single block entity, if at all (Loisel et al., 2021). This points to an urgent need to better understand what level of detail is needed to characterize the heterogeneous boreal landscapes and their response to warming.

To fill these research gaps, we conducted an in-depth study in a typical northern boreal landscape located in northern Finland. We performed a high-resolution land cover classification based on multi-source remote sensing and field data. We collected large amounts of LCT-specific data including ecosystem-atmosphere fluxes of CO₂ and CH₄, soil and vegetation properties, and meteorological and hydrological variables. With these data, we calibrated and validated terrestrial and aquatic biogeochemical models, and simulated daily greenhouse gas (GHG) fluxes under present and future conditions. In addition, we estimated the potential development of the radiative effect of these fluxes. With these analyses, we aim to quantify the heterogeneity in peatland C dynamics and their radiative effect relative to that in the landscape scale and demonstrate the importance of accurately mapping the small-scale variation in peatland types within a typical boreal landscape. To assess the need for improved peatland mapping within the boreal zone, we surveyed how accurately the peatlands within the study area are depicted in current global, continental, and national land cover products.

2 Materials and methods

2.1 Study area

This study was conducted in a 32.8 km² northern boreal catchment situated in northern Finland (69.13-69.26°N, 27.21-27.45°E; 155 m a.s.l), about 200 km south of the Arctic Ocean (Figure 1). The catchment is characterized by subarctic climate (Aurela, Laurila, & Tuovinen, 2001). The mean annual air temperature during the period from 1981 to 2010 at the Inari Ivalo weather station (59 km south of Kaamanen) was -0.4 °C, with the warmest and coldest monthly air temperature being 14.0 °C and -12.8 °C in July and January, respectively (Pirinen et al., 2012). During the aforementioned period, the mean annual precipitation was 472 mm, and the mean annual relative humidity was 79% (Pirinen et al., 2012).

2.2 Land cover classification

Land cover in the study area was classified using a geographic object-based image analysis approach, following the methodology described by Räsänen, Juutinen, Tuittila, Aurela, and Virtanen (2019) and Räsänen and Virtanen (2019). Object-based approaches have been documented to be effective in particular when analyzing high-spatial resolution remote sensing imagery (Blaschke et al., 2014; Chen, Weng, Hay, & He, 2018), and it has been shown that inclusion of multi-source (*i.e.*, multiple types of remote sensing data) and multi-temporal remote sensing data increases land cover classification accuracy (Amani et al., 2017; Chasmer et al., 2020; Halabisky, Babcock, & Moskal, 2018; Karlson et al., 2019; Räsänen & Virtanen, 2019). Specifically, a WorldView-2 satellite image (WV-2, DigitalGlobe Inc., Westminster, CO, USA) was segmented with a full lambda schedule segmentation with an average segment size of 0.2 ha. For each segment, 352 features, including spectral, topographic, vegetation

height, and texture features, were calculated from the WorldView-2 image, four PlanetScope satellite images (PS, Planet Labs Inc., San Francisco, CA, USA) from different phenological stages and aerial lidar data (National Land Survey of Finland) (Table S1).

Training data were collected from 16 transects of 0.25-1.0 km in length and visual interpretation of an aerial orthophoto. In total, there were 1058 training segments (18-383 in each LCT). A supervised random forest classification (Breiman, 2001) was used to classify 11 LCTs (excluding streams) (Table 1; Figure S1). Accuracy of the classification was assessed with a pixel-based approach utilizing 359 vegetation plots, of which 137 were circular plots with a radius of 5 m (of which 59 were in transects, and 78 randomly sampled), 204 were quadrats with a 50 cm side length (in transects), and 18 were circular plots with a radius of 20 cm (Räsänen & Virtanen, 2019).

After the random forest classification, the stream LCT was added to the map from National Land Survey of Finland topographic database. Owing to large differences in hydrology and C dynamics (Figures S2-S7; Table S2), the fen string LCT was split into string top and string margin fractions by assuming that 59.2% of the string belong to tops and 40.8% to margins as per the land cover classification conducted for a peatland area within the landscape (Heiskanen et al., 2021; Räsänen & Virtanen, 2019) (Table 2).

2.3 Flux measurements

The ecosystem-atmosphere fluxes of CO₂ and CH₄ were measured on the dominant peatland surfaces, *i.e.*, pine bog, string top, string margin, tall sedge fen, and flark fen, using a static chamber technique (Heiskanen et al., 2021; Juutinen et al., 2013; Laine, Riutta, Juutinen, Väliranta, & Tuittila, 2009). The measurements were made repeatedly during the growing seasons 2005, 2006, 2017, and 2018 (Heiskanen et al., 2021; Juutinen et al., 2013; Laine et al., 2009). Permanent chamber bases were installed in replicate for each peatland type.

Net ecosystem CO₂ exchange (NEE) was measured using transparent chambers equipped with a fan and an infra-red gas analyzer (in 2005-2006, EGM-3, PP-systems, MA, USA; in 2017-2018, Picarro G2401, Picarro Inc., CA, USA), and was determined from several (2-4) replicate measurements. Ecosystem respiration (ER) was measured using opaque chambers. Fluxes were calculated from concentration changes using standard methods (Heiskanen et al., 2021; Juutinen et al., 2013; Laine et al., 2009). Gross primary productivity (GPP) was calculated as the difference between NEE and ER. Positive fluxes in this study indicate a C flux to the atmosphere, while negative values represent C uptake by the ecosystem.

In 2005-2006, the CH₄ fluxes were determined in aluminum chambers equipped with a fan, and CH₄ concentration was measured using gas chromatographs (HP-5710A and HP-5890A, Palo Alto, CA, USA) equipped with a flame ionization detector (Juutinen et al., 2013). In 2017-2018, the CH₄ flux measurements were conducted with the CO₂ chamber flux set-up.

In the pine forest (69.1°N, 27.3°E), NEE was measured using the eddy covariance (EC) technique from June 2017 to December 2018 (Heiskanen et al., 2021). The NEE data for birch forest were derived from the EC measurements conducted at Petsikko (69.28°N, 27.14°E) in June–September 1996 (Aurela, Tuovinen, & Laurila, 2001).

At a lake within the study landscape, the CO₂ and CH₄ fluxes were measured manually with a Picarro G2401 (Picarro Inc., CA, USA) and floating chambers during the summer season (June–August) of 2017 (Juutinen et al., 2013).

2.4 Terrestrial ecosystem modeling

Ecosystem C dynamics of the terrestrial land cover types in the study landscape were simulated using a process-based biogeochemistry model, NEST-DNDC (Zhang, Sachs, Li, & Boike, 2012). It integrates a widely used biogeochemical model DeNitrification-DeComposition (DNDC) (Kou et al., 2020; Li, Aber, Stange, Butterbach-Bahl, & Papen, 2000) with the Northern Ecosystem Soil Temperature model (NEST) (Zhang, Chen, & Cihlar, 2003). Thus, the model can effectively simulate C dynamics in LCTs of the cold circumpolar regions (Deng et al., 2017; Treat et al., 2018; Zhang et al., 2012). In the model, all LCTs share common climate and atmospheric environmental conditions (*e.g.*, atmospheric CO₂ and nitrogen (N) concentration), but they differ in their assigned land types, soil, and vegetation characteristics. Therefore, the model is particularly suitable to work with ecosystem C dynamics in fragmented circumpolar landscapes (Zhang et al., 2012).

In this study, the simulations with the NEST-DNDC model for the terrestrial LCTs were conducted through the following three steps. First, the datasets required for model input were prepared, including data associated with climate, soil, and vegetation. Of them, the climate dataset, shared by all LCTs, include historical meteorological observations for 1996 and 2005-2018, and future data for 2019-2099. The historical climate dataset, including daily mean, maximum, and minimum air temperatures, precipitation, wind speed, global radiation, and relative humidity, were derived from the Utsjoki Kevo weather station (69.8°N, 27.0°E) of the Finnish Meteorological Institute. The future climate data was extracted from the bias-corrected dataset of the International Impact Model Intercomparison Project (ISIMIP) output from HadGEM2-ES (Frieler et al., 2017).

The LCT-specific soil variables that were used to drive the model consisted of texture, bulk density, pH, soil C concentration, and soil C:N ratio (Table S2). The soil texture was loamy sand for forests and pristine peat for peatlands. In all peatlands, soil samples of a known volume were collected from layers 0–5 cm and 15–20 cm beneath the litter layer (the layer where vascular plant and moss leaf structures are still discernible) using a knife and scissors. The samples were dried (48 h at 75 °C) and weighted for dry mass. Bulk density was calculated based on the volume and dry mass of the samples. Parts of dry samples were ground using a ball mill and 0.2 g subsamples of ground material were analyzed for total C and N concentrations using a LECO CNS-2000 analyzer (LECO Corporation, Saint Joseph, MI, USA). Soil pH was estimated in the field in water collected at the depth of 30 cm. In models, means of the two peat layers were used for bulk density, C concentration, and C:N ratio. In pine, birch and pine-birch mixed forests, pits were dug to a depth of 100 cm and horizontal soil cores (length 5

cm, diameter 3 cm) were collected from the organic (O) and eluvial (E) horizons, from the top and bottom parts of the illuvial (B) horizon, and at the depth of 50 and 100 cm. These samples were analyzed following the procedures described for peatland samples except that the pH was measured from O horizon samples and samples collected at 30 cm depth in distilled water solution. In models, means of values of all available soil horizons were used for forest soil bulk density, C concentration, C:N ratio, and pH. Vegetation data included in the models consisted of aboveground plant biomass and leaf area index (LAI) of different LCTs (Tables S3-S4). The aboveground biomass and LAI of each LCT was determined based on 130 circular plots with a 5 m radius (71 random plots, 59 plots in transects) distributed among the LCTs (see Supplementary Text for detailed information).

Second, we calibrated and validated the model for different LCTs (Figures S2-S15). The observed C fluxes used for the model calibration included the 1996 data of birch forest, the 2006 data of pine bog, string margin, tall sedge fen, and flark fen, and the 2017 data of string top and pine forest. The calibrated models were then validated with the remaining C flux data, from 2005 for pine bog, string margin, tall sedge fen, and flark fen, from 2017 for string margin, and from 2018 for string top, string margin, and pine forest. Finally, we ran the calibrated and validated model for the period 2005-2018 for the dominant terrestrial LCTs. To explore the potential trajectory of RE heterogeneity under warming, we then drove the model for the period 2019-2099 with variable temperature from two Representative Concentration Pathway scenarios, RCP4.5 and RCP8.5, keeping other climatic and atmospheric inputs constant (2005-2018 averages) (Lucht et al., 2002). The C budget of mixed forest and open forest was simulated based on parameters from pine/birch forest and their own soil and vegetation

data. The pine bog simulation was also used for birch swamp (covering only 0.12% of study area) in the landscape-scale estimation of C budget and RE since observations were lacking for birch swamp.

2.5 Aquatic ecosystem modeling

The Arctic Lake Biogeochemistry Model (ALBM), which is a one-dimensional process-based climate-sensitive lake biogeochemistry model, was used to simulate the CO₂ and CH₄ fluxes from lakes in the study area (Guo et al., 2020; Tan, Zhuang, & Anthony, 2015; Tan et al., 2017). For lake C fluxes, the model simulates both the diffusive and the ebullitive emission. The model was first calibrated against observations of water temperature and C fluxes of the lake using the Monte Carlo method with 10,000 parameter sample sets. The optimum parameter set was then selected based on the total root-mean-square error of the modeled CO₂ and CH₄ fluxes. Finally, we run simulations over the same period forced by the same meteorological data as for the other LCTs (Figure S16). The lake simulation was also used for streams in the landscape-scale estimation of C budget and RE.

2.6 Radiative effect of greenhouse gas fluxes

The annual CO₂ and CH₄ flux densities (g m⁻² yr⁻¹) of each LCT during the period of 2005-2099 were used as input to estimate the radiative effect (RE) of these fluxes, *i.e.*, their contribution to Earth's radiative balance. We expressed this effect as the cumulative RE due to an annual emission or uptake pulse over time horizons of 25 and 100 yr, which was calculated using a dynamic radiative forcing (RF) model (Lohila et al., 2010; Mathijssen et al., 2017; Piilo et al., 2020). Even though we used a RF model here, it is important to note that we refer to this quantity as RE, as it does not represent

a forcing that would result from a perturbation to Earth's energy balance (Neubauer, 2021). This modelling is performed in order to obtain a common metric for the CO₂ and CH₄ fluxes, in a similar vein to the CO₂-equivalent fluxes derived from the global warming potential concept; however, using RE as the common metric provides additional flexibility as we can dynamically account for the effect of changing background concentrations.

In the RF model, CO₂ and CH₄ pulses were assumed to be instantaneously and completely mixed in the atmosphere (Myhre et al., 2013). The resulting atmospheric concentration pulses were modeled to decay according to characteristic time scales related to global biogeochemical cycles. For CO₂, these dynamics were implemented as a weighted sum of four exponential functions, where the shortest perturbation time was 4.3 yr and the slowest decay function effectively corresponded to a permanent atmospheric change for 22% of each annual pulse (Joos et al., 2013). The evolution of the atmospheric CH₄ concentration perturbation was calculated as an exponential decay with a single atmospheric perturbation time scale of 12.4 yr (Myhre et al., 2013).

The annual emission/uptake pulses were integrated over time by accounting for their timing and decay, resulting in time series of atmospheric CO₂ and CH₄ concentration changes. Atmospheric oxidation of the emitted CH₄ molecules to CO₂, which generates an indirect RE, was included in the model assuming an 80% efficiency for the CH₄-to-CO₂ conversion (Boucher, Friedlingstein, Collins, & Shine, 2009). The instantaneous RE resulting from the modeled CO₂ and CH₄ concentration changes was calculated with a radiative efficiency parameterization (Etminan, Myhre, Highwood, & Shine, 2016). This parameterization takes into account the spectral interactions between CO₂, CH₄,

and nitrous oxide. The model also includes an estimate for the indirect CH₄-induced RE due to ozone and stratospheric water vapor changes (Myhre et al., 2013). The RE due to ecosystem-atmosphere fluxes was calculated as a marginal change with respect to specified, variable background concentrations (Lohila et al., 2010). These concentrations were adopted from the RCP scenarios (Meinshausen et al., 2011). In this study, the total RE refers to the sum of the RE due to CO₂ and CH₄.

2.7 Statistical analysis

The landscape-scale C budget and RE were estimated by weighting the C budget and RE of each LCT (except non-vegetated) with the corresponding relative area within the catchment. The role of peatlands in the landscape-scale heterogeneity in C budget and RE was quantified at two levels, based on the LCT-specific C fluxes expressed (1) per unit area ('LCT-based heterogeneity') and (2) as area-weighted budgets ('area-based heterogeneity'). For the LCT-based heterogeneity, we calculated the Sum of Squared Deviations (SSD) from the arithmetic mean among peatland LCTs and that among all LCTs within the landscape and then divided the peatland SSD by the landscape SSD. For the area-based heterogeneity, we calculated the ratio between the SSD from the area-weighted mean among peatland LCTs and that among all LCTs within the boreal landscape.

To illustrate the uncertainty in the landscape-scale results due to aggregation or misclassification of peatlands, we tested the statistical difference among different land cover scenarios (*i.e.*, scenarios that peatlands are combined, and scenarios that peatlands are mis-classified as non-peatland LCTs) with Least Significant Difference (LSD). Combining peatland LCTs is relevant because peatland LCTs in the current

circumpolar peatland maps are generally expressed as a uniform land cover type (Hugelius et al., 2020; Xu, Morris, Liu, & Holden, 2018), without capturing spatial heterogeneity among different peatland types. In remote sensing-based products, peatlands can also be confused with other terrestrial or aquatic LCTs. Most commonly, forested peatland is mis-classified as forest (Thompson et al., 2016) and open waterlogged peatland with low vegetation as a lake (Matthews et al., 2020).

When estimating potential trajectories of RE heterogeneity among different LCTs under future warming scenarios, the relative importance of CO₂ and CH₄ in explaining the trend of total RE heterogeneity was analyzed with the random forest technique (Delgado-Baquerizo et al., 2018).

2.8 Survey of land cover products

We surveyed seven widely used global land cover products in our study area and assessed how well peatlands are presented in them by calculating the fractional peatland/wetland area and estimating the spatial agreement with our LCT data by error matrices (Frey & Smith, 2007; Krankina et al., 2008). Moreover, we included in the comparison one continental and one national land cover product. The nine products considered are detailed in Table 3.

3 Results

3.1 Landscape heterogeneity

Twelve LCTs were distinguished within the studied boreal landscape with high spatial resolution land cover classification (Figures 1, S1; Tables 1-2), with an overall accuracy of 73.1% (Table S5). Four of these LCTs were forests (*i.e.*, pine, birch, mixed, and open

forests, occupying 60.6% of the landscape), two were water bodies (*i.e.*, lake and stream, 13.2%), one represents non-vegetated areas (0.7%), and five were peatlands (25.5%) that were distributed along a gradient from forests to water bodies (Table 1). Among the peatland LCTs, pine bog (9.3%), birch swamp (0.1%), and fen string (including thin, elongated, and smaller, rounded elevated microforms; 2.7% string top and 1.8% string margin) were characterized as dry communities as their water tables were below the peat surface (Tables 2, S2). Of these, pine bog and birch swamp represent forested dry peatlands while string top and margin represent open dry peatland habitats (Table 1). The two water-logged peatland LCTs, *i.e.*, tall sedge fen (5.6%) and flark fen (6.0%), represent open wet peatland habitats (Tables 1-2, S2).

3.2 Carbon budget under present climate

The various LCTs differ in vegetation, soil, and hydrological characteristics (Figures S2-S16; Tables 1, S2-S4), leading to heterogeneity in the ecosystem-atmosphere fluxes of CO₂ and CH₄ (Figure 2). For the total C budget (sum of CO₂-C and CH₄-C budgets), the terrestrial LCTs (peatlands and forests) functioned as C sinks, while lakes functioned as a significant C source (mean \pm 95% confidence interval: 27 ± 2 g C m⁻² yr⁻¹) during the period 2005-2018 (Figure 2a). Among the peatland LCTs, the C budget ranged from a large C sequestration in pine bog (-141 \pm 17 g C m⁻² yr⁻¹) to a small sequestration in tall sedge fen (-17 \pm 3 g C m⁻² yr⁻¹), while among the forest types, the largest C sink was found for pine forest (-154 \pm 17 g C m⁻² yr⁻¹) and the smallest for open forest (-45 \pm 6 g C m⁻² yr⁻¹) (Figure 2a). The variability and magnitude of the total C budget was dominated by CO₂ (Figure 2b). Most peatland LCTs emitted CH₄ to the atmosphere, with the largest emission from the water-logged peatland LCTs (tall sedge fen: 19 \pm 1 g C m⁻² yr⁻¹; flark fen: 17 \pm 2 g C m⁻² yr⁻¹) (Figure 2e). Forests functioned

as weak CH₄ sinks (-0.23 \pm 0.02 to -0.26 \pm 0.02 g C m⁻² yr⁻¹), while lakes were CH₄ sources (1.33 \pm 0.09 g C m⁻² yr⁻¹) (Figure 2e).

By quantifying the role of peatlands in the landscape-scale heterogeneity in C budget at the LCT level, we found that the variability in the total C mass budget among peatland LCTs accounted for 38 ± 5 % of the variability due to all landscape LCTs combined (Figure 2f). The CO₂-C budget, GPP, and ER heterogeneity had a similar peatland contribution (33 ± 5 %, 36 ± 1 %, and 39 ± 2 %, respectively) (Figure 2f). Compared to them, peatlands explained a significantly larger part of the variability (81 \pm 0.5 %) in the CH₄-C budget (Figure 2f).

The landscape-scale C budget, obtained by weighting the CO_2 and CH_4 exchange rates of each LCT by the corresponding areas (Table 2), was -106 \pm 11 g C m⁻² yr⁻¹ in 2005-2018. It was dominated by the CO_2 uptake of -108 \pm 10 g C m⁻² yr⁻¹ while the CH_4 emission was 2.28 \pm 0.19 g C m⁻² yr⁻¹ (landscape mean in Figure 2a-e). Peatlands explained a smaller part of the variability in total C budget (19 \pm 3 %), CO_2 -C budget (15 \pm 3 %), CO_2 -C budget (Figure 2g). These proportions were also less than the proportion of the total peatland area within the landscape (26%) (Table 2). However, peatlands explained as much as 88 \pm 0.1 % of the CH_4 flux variability when scaling them with LCT areas (Figure 2g).

3.3 Radiative effect of present carbon budget

The different heterogeneities in CO₂-C and CH₄-C budgets, together with the different radiative impacts of CO₂ and CH₄ (Myhre et al., 2013), led to a further layer of LCT

heterogeneity in the C flux effect on radiative balance (Figure 3). The total RE generated by CO₂ and CH₄ fluxes varied greatly among the peatland LCTs (Figure 3a). Specifically, pine bog had the greatest negative RE (-37 \pm 4 fW m⁻² over the 100-yr time horizon, 1 fW = 10⁻¹⁵ W), followed by string top (-25 \pm 3 fW m⁻²). In contrast, tall sedge fen exhibited the largest positive RE among all the LCTs (69 \pm 6 fW m⁻²), followed by flark fen (52 \pm 7 fW m⁻²). Consequently, the RE generated by different peatland types spanned a range of 107 \pm 9 fW m⁻², which was more than twice that among the forest and aquatic LCTs (56 \pm 5 fW m⁻²) (Figure 3a).

Despite comprising just 26% of the landscape area, the variability among peatland types accounted for 77 ± 3 % to 81 ± 1 % of the total variability in RE at the LCT level and 65 ± 4 % to 79 ± 2 % when considering LCT areas, depending on the time horizon (Figure 3d-e). These were similar to the corresponding SSD ratio for the CH₄-C budget (LCT-based: 81 ± 0.5 %; area-based: 88 ± 0.1 %) and much larger than those for the CO₂-C budget (LCT-based: 33 ± 5 %; area-based: 15 ± 3 %) (Figure 3d-e).

3.4 Uncertainty due to biased peatland classification

The area-weighted total RE resulting from the CO₂ and CH₄ budgets was -20 \pm 3 fW m⁻² per unit area of the region over the 100-yr time horizon (CO₂: -30 \pm 3 fW m⁻²; CH₄: 10 ± 1 fW m⁻²; landscape mean in Figure 3a-c).

Using this result as a baseline (Scenario 1, Figure 4), we analyzed the potential deviation in RE for scenarios in which peatland LCTs were combined (Scenario set 2 in Figure 4) or mis-classified as forests or lakes (Scenario set 3 in Figure 4). Regarding

scenarios in which peatland LCTs are combined, our results showed that the negative RE over the 100-yr time horizon significantly decreased when all the peatland LCTs were pooled into the forested dry peatland class (pine bog, -32 ± 3 fW m⁻², Scenario 2a) or treated as string top (-29 ± 3 fW m⁻², Scenario 2b) (Figure 4a). On the other hand, the negative RE significantly increased when all the peatland LCTs were classified as water-logged peatland (tall sedge fen, -5 ± 3 fW m⁻², Scenario 2d; flark fen, -10 ± 4 fW m⁻², Scenario 2e) (Figure 4a). This suggests that, to accurately estimate the regional RE, the LCT mapping must be able to distinguish between the water-logged and dry peatland areas within the landscape. Consistent with this point, when all the water-logged peatland areas were classified as tall sedge fen and all the dry peatland LCTs were classified as string top, RE did not change significantly (Scenario 2f, Figure 4a).

Regarding scenarios that peatlands are confused with other terrestrial or aquatic LCTs, our results showed that the uncertainty in RE was insignificant if pine bog (the dominant forested peatland in the landscape) was identified as pine forest (-21 ± 4 fW m⁻², Scenario 3a, Figure 4a). This was associated with the comparable CO₂ budgets and the consistently small CH₄ emissions of the forested peatlands and their corresponding forest types (Figure 2). Similarly, when flark fen, an open water-logged peatland with low vegetation cover, was classified as a lake, the modeled RE did not change significantly (Scenario 3b, Figure 4a). However, when the two above-mentioned misclassification scenarios were adopted simultaneously and the remaining open peatland LCTs were represented by a single open dry peatland type (string top), the negative RE decreased significantly (Scenario 3c, Figure 4a). Our results demonstrate the potentially high sensitivity of the modeled RE to peatland classification (Figure 4a).

Further analyses showed that over a shorter time horizon (25 yr) this sensitivity involved not only the magnitude but also the sign of RE (Figure 4b).

Like RE, our results also demonstrated that the aggregation or misclassification of peatlands could significantly alter the estimated landscape-scale C budget, although the differences among various scenarios were smaller compared to RE (Figure 4c). Moreover, we found that the landscape-scale CO_2 budget and its RE did not differ significantly (p > 0.05) from those calculated with the full LCT classification (Scenario 1) in any peatland aggregation or misclassification scenario (Figure 4d-f). In contrast, there were significant differences in the landscape-scale CH_4 budget and its RE among different scenarios (Figure 4d-f).

3.5 Radiative effect of future carbon budget

Based on our RE calculations with the LCT fluxes modeled until 2099, we found that the variation in total RE due to the C budget of different peatland LCTs significantly increased during 2005-2099 under both RCP scenarios considered (p < 0.001; Figure 5a-b). Even though the radiative efficiency (*i.e.*, RE per atmospheric GHG change) is concurrently reduced as background concentrations increase (Etminan et al., 2016; Meinshausen et al., 2011), the warming-induced changes in GHG fluxes resulted in an amplified variability in the RE of total C budget among peatland LCTs. Compared to the present period (2005-2018), the peatland heterogeneity in total RE during 2086-2099 was enhanced by 143% under RCP4.5 and by 243% under RCP8.5 (Figure 5a-b). Moreover, the SSD of total RE among all the landscape LCTs also significantly increased under the two RCP scenarios (p < 0.001; Figure 5a-b), indicating an amplified

heterogeneity in RE at the landscape scale as well. Similar to the total RE, the SSD of CH₄-induced RE among the peatland LCTs significantly increased with warming under both climate change scenarios (p < 0.001; Figure 5c-d). Moreover, our results showed that, compared to CO₂-C exchange, the RE heterogeneity due to CH₄-C budget had a larger relative importance in explaining the trend of total RE heterogeneity among peatlands during 2005-2099 (Figure 5e-f).

3.6 Survey of different land cover products

Compared to the 25.5% areal coverage of peatlands within the Kaamanen landscape revealed by our classification, there was no peatland/wetland specified in the global land cover map of GLCC, MODIS.LCT or GLWD; the coverage was 0.1% in both GlobCover2009 and FROM-GLC10, as high as 58.0% in GLC2000, and 24.8% in PEATMAP (Figure 6; Table 3). Although the proportion of peatlands was similar in PEATMAP and this study, the spatial agreement between their areas was only 48.5% (Table 3). The corresponding spatial agreement for GLC2000, GlobCover2009, and FROM-GLC10 were 21.8%, 0.1%, and 0.01%, respectively (Table 3). Regarding the peatland/wetland heterogeneity, there was only one peatland/wetland type defined in any of the considered global products including such a LCT, *i.e.*, 'regularly flooded shrub and/or herbaceous cover' in GLC2000, 'closed to open (>15%) grassland or woody vegetation on regularly flooded or waterlogged soil' in GlobCover2009, 'wetland' in FROM-GLC10, and 'peatland' in PEATMAP (Figure 6).

The European-level product, CLC2018EU.25ha, has a similar peatland representation to PEATMAP, *i.e.*, one peatland category ('peatbog'), with a 25.3% areal coverage and

44.8% spatial agreement (Figure 6; Table 3). Unlike the larger scale products, the national data base CLC2018FI.20m provides multiple peatland classes for the Kaamanen landscape ('Broad-leaved forest on peatland', 'Coniferous forest on peatland', 'Mixed forest on peatland', 'Transitional woodland/shrub cc 10-30% on peatland' (cc = canopy closure), 'Peatbog', 'Terrestrial inland marsh', and 'Aquatic inland marsh'), with a relatively accurate peatland area (28.6%) and a high score of spatial agreement (62.0%) (Figure 6; Table 3). On the other hand, the 'Peatbog' class, which in CLC2018FI.20m is defined as open peatlands smaller than 25 ha (https://ckan.ymparisto.fi/dataset/corine-maanpeite-2018), alone occupied about 84% of the total peatland/wetland area (Figure 6). This indicates that, although there are multiple peatland/wetland classes and forested peatlands are separated from forests and open peatlands, there is no separation of small peatland patterns in CLC2018FI.20m either.

4 Discussion

This study couples a detailed land cover classification of a typical boreal landscape with quantification of spatial heterogeneity in C budget and its climate impact (RE); based on these comprehensive data, we assessed the effect of peatland classification accuracy on C budget and RE, derived potential trajectories of RE heterogeneity under future warming conditions and surveyed peatland representation in global land cover products. This was motivated by the fact that landscapes including peatlands are widespread across the boreal biome. By overlaying two maps, *i.e.*, the map of terrestrial ecoregions of the world (Olson et al., 2001) and the latest northern peatland map with 10-km pixels (Hugelius et al., 2020), we find that there are approximately 150,400 10-km pixels within the boreal zone, of which 140,700 (*i.e.*, 94%) contain peatlands

(peatland area fraction > 0) (Figure S17a). Our results jointly advocate the detailed delineation of peatland heterogeneity, *i.e.*, determining a sufficient number of LCTs with differing characteristics, so that we can reduce uncertainties in C budget estimates of the boreal biome. This conclusion is further supported by previous studies that focused on individual boreal peatland ecosystems (Heiskanen et al., 2021; Li et al., 2016; Lund et al., 2010).

Indeed, recently, there have been multiple attempts to produce local, regional, national, and circumpolar databases of northern peatlands. In part of these attempts, however, all peatlands and wetlands have been lumped into one class (Hird, DeLancey, McDermid, & Kariyeva, 2017; Hugelius et al., 2020; Karlson et al., 2019; Tanneberger et al., 2017; Xu et al., 2018), but there exist approaches that include separate classes for different peatland types (Amani et al., 2017; Bourgeau-Chavez et al., 2017; Korpela, Haapanen, Korrensalo, Tuittila, & Vesala, 2020; Mahdianpari et al., 2020; Olefeldt et al., 2021; Räsänen & Virtanen, 2019). Currently, the most detailed circumpolar database uses existing GIS datasets and machine learning modeling to estimate the fractional coverage of five different wetland classes in 0.5° grid cells (Olefeldt et al., 2021). Also some other data products have relied on existing GIS databases (Hugelius et al., 2020; Tanneberger et al., 2017; Xu et al., 2018), while others have used remotely sensed data that enable construction of higher spatial resolution datasets (Amani et al., 2017; Bourgeau-Chavez et al., 2017; Hird et al., 2017; Karlson et al., 2019; Mahdianpari et al., 2020; Räsänen & Virtanen, 2019).

To generate locally accurate maps of peatland LCTs, it has been shown that ultra-high spatial resolution (pixel size < 1 m) airborne or drone data are required (Korpela et al.,

2020; Räsänen & Virtanen, 2019). Nevertheless, the use of such data is presently impossible for large regions, but maps based on high-resolution satellite data (pixel size < 30 m) are, at least in some cases, sufficient to predict the proportional area of different LCTs (Bartsch, Hofler, Kroisleitner, & Trofaier, 2016; Mahdianpari et al., 2020; Treat et al., 2018). In practice, however, even the national-scale land cover product (CLC2018FI.20m), while showing possible guidelines for larger scale maps and the best performance of the products compared in this study, depicts peatlands at much coarser than the nominal 20-m pixel level.

Both at small and large scales, peatland LCT detection requires multiple remote sensing data sources that bring complementary information, including, *e.g.*, optical data depicting spectral properties of land cover, lidar data providing information about topography and vegetation structure, and synthetic aperture radar (SAR) data sensitive to moisture and surface structure (Amani et al., 2017; Bourgeau-Chavez et al., 2017; Hird et al., 2017; Karlson et al., 2019; Mahdianpari et al., 2020; Räsänen, Manninen, Korkiakoski, Lohila, & Virtanen, 2021; Räsänen & Virtanen, 2019). Freely available high-resolution remote sensing datasets, such as Sentinel-1 SAR, optical Sentinel-2 and Landsat 8, and ArcticDEM topographic data would enable the generation of circumpolar maps of peatland LCTs. Such maps could be upscaled from local peatland maps and field inventories; vice versa, circumpolar maps could be downscaled to locally accurate products with high resolution datasets, such as airborne or drone lidar and hyperspectral data.

Besides the large spatial heterogeneity, boreal peatlands can also vary temporally under environmental changes. Our modeling results showed that the LCT-based RE

heterogeneity among peatland types could be enhanced in future warming conditions, suggesting that peatland heterogeneity in climate feedback to C fluxes would change with environmental changes irrespective of land cover change. The reason why we did not consider changes in peatland area or LCT distribution within the Kaamanen landscape is that paleoecological evidence indicates that there has not been any major changes in the surface microtopography and vegetation taxonomic composition since the formation of the irregular string and flark pattern ca. 1000 yr ago (Piilo et al., 2020). Furthermore, there is no permafrost within the study area (Aurela, Laurila, et al., 2001), and hence permafrost thawing, which could induce drastic changes in peatland types and distribution (Helbig et al., 2017; Johansson et al., 2006; Payette, Delwaide, Caccianiga, & Beauchemin, 2004), has no effect there. However, as 77% of the 10-km peatland pixels of the boreal map do contain permafrost (Figure S17b), the heterogeneity of peatlands potentially increases across the northern boreal landscape with permafrost thawing. Overall, vegetation and hydrology changes affecting the peatland distribution and characteristics within the boreal zone cannot be ruled out. These potential changes under environmental changes highlight not only the delineation of the spatial heterogeneity of peatlands, but also their temporal dynamics.

613

614

615

616

617

618

619

620

596

597

598

599

600

601

602

603

604

605

606

607

608

609

610

611

612

5 Conclusions

Based on an extensive set of field data including CO_2 and CH_4 fluxes, soil and vegetation characteristics, and an explicit land cover classification, we modeled the C budgets and their radiative climate effects both for the boreal landscape and its individual LCTs. The average present-day, landscape-scale budgets of CO_2 and CH_4 were -108 \pm 10 and 2.3 \pm 0.2 g C m⁻² yr⁻¹, respectively. We show that, despite only comprising 26% of the study area, peatlands within the Kaamanen boreal landscape

account for 88% of the area-based heterogeneity in CH₄-C budget, and 65% and 79% of that in the total radiative effect over the 100-yr and 25-yr time horizons, respectively. Misclassifying peatlands or inadequately representing the heterogeneity among the peatland types can alter the magnitude of the modeled radiative effect significantly over the 100-yr time horizon, and even change the sign over the 25-yr time horizon. Warming tends to enhance the RE heterogeneity of peatland C budgets. We also observed that global land cover products have obvious biases in their classification of boreal peatlands. Overall, this study implies the great significance of resolving land cover specifics, especially peatland heterogeneity, in sufficient detail across the boreal biome for constraining the circumpolar C-climate nexus.

References

631

632 Åberg, J., Jansson, M., & Jonsson, A. (2010). Importance of water temperature and thermal stratification dynamics for temporal variation of surface water CO₂ in a boreal lake. 633 634 Journal of Geophysical Research: Biogeosciences, 115(G2). doi:https://doi.org/10.1029/2009JG001085 635 Amani, M., Salehi, B., Mahdavi, S., Granger, J. E., Brisco, B., & Hanson, A. (2017). Wetland 636 classification using multi-source and multi-temporal optical remote sensing data in 637 Newfoundland and Labrador, Canada. Canadian Journal of Remote Sensing, 43(4), 638 360-373. doi:10.1080/07038992.2017.1346468 639 Arino, O., Ramos Perez, J. J., Kalogirou, V., Bontemps, S., Defourny, P., & Van Bogaert, E. 640 641 (2012). Global Land Cover Map for 2009 (GlobCover 2009). Retrieved from: https://doi.org/10.1594/PANGAEA.787668 642 643 Aurela, M., Laurila, T., & Tuovinen, J. P. (2001). Seasonal CO₂ balances of a subarctic mire. 644 Journal ofGeophysical Research-Atmospheres, 106(D2),1623-1637. 645 doi:10.1029/2000jd900481 Aurela, M., Lohila, A., Tuovinen, J. P., Hatakka, J., Penttila, T., & Laurila, T. (2015). Carbon 646 647 dioxide and energy flux measurements in four northern-boreal ecosystems at Pallas. 648 Boreal Environment Research, 20(4), 455-473. 649 Aurela, M., Tuovinen, J. P., & Laurila, T. (2001). Net CO₂ exchange of a subarctic mountain birch ecosystem. Theoretical and Applied Climatology, 70(1-4), 135-148. 650 doi:10.1007/s007040170011 651 652 Bartholomé, E., & Belward, A. S. (2005). GLC2000: a new approach to global land cover mapping from Earth observation data. *International Journal of Remote Sensing*, 26(9), 653 1959-1977. doi:10.1080/01431160412331291297 654 Bartsch, A., Hofler, A., Kroisleitner, C., & Trofaier, A. M. (2016). Land cover mapping in 655 northern high latitude permafrost regions with satellite data: achievements and 656 657 remaining challenges. Remote Sensing, 8(12). doi:10.3390/rs8120979

- 658 Blaschke, T., Hay, G. J., Kelly, M., Lang, S., Hofmann, P., Addink, E., . . . Tiede, D. (2014).
- 659 Geographic Object-Based Image Analysis Towards a new paradigm. ISPRS Journal
- of Photogrammetry and Remote Sensing, 87, 180-191.
- doi:https://doi.org/10.1016/j.isprsjprs.2013.09.014
- Boucher, O., Friedlingstein, P., Collins, B., & Shine, K. P. (2009). The indirect global warming
- potential and global temperature change potential due to methane oxidation.
- Environmental Research Letters, 4(4), 044007. doi:10.1088/1748-9326/4/4/044007
- Bourgeau-Chavez, L. L., Endres, S., Powell, R., Battaglia, M. J., Benscoter, B., Turetsky, M.,
- 666 ... Banda, E. (2017). Mapping boreal peatland ecosystem types from multitemporal
- radar and optical satellite imagery. Canadian Journal of Forest Research, 47(4), 545-
- 668 559. doi:10.1139/cjfr-2016-0192
- Bradshaw, C. J. A., & Warkentin, I. G. (2015). Global estimates of boreal forest carbon stocks
- 670 and flux. Global and Planetary Change, 128, 24-30.
- doi:10.1016/j.gloplacha.2015.02.004
- 672 Breiman, L. (2001). Random forests. Machine Learning, 45(1), 5-32.
- doi:10.1023/a:1010933404324
- 674 Chapin III, F. S., Matson, P. A., & Vitousek, P. (2011). Principles of Terrestrial Ecosystem
- 675 Ecology. New York, USA: Springer Science & Business Media.
- 676 Chasmer, L., Cobbaert, D., Mahoney, C., Millard, K., Peters, D., Devito, K., . . . Niemann, O.
- 677 (2020). Remote sensing of boreal wetlands 1: data use for policy and management.
- 678 Remote Sensing, 12(8), 1320. doi:10.3390/rs12081320
- 679 Chen, G., Weng, Q., Hay, G. J., & He, Y. (2018). Geographic object-based image analysis
- 680 (GEOBIA): emerging trends and future opportunities. GIScience & Remote Sensing,
- 681 55(2), 159-182. doi:10.1080/15481603.2018.1426092
- 682 Chi, J., Nilsson, M. B., Laudon, H., Lindroth, A., Wallerman, J., Fransson, J. E. S., . . . Peichl,
- 683 M. (2020). The Net Landscape Carbon Balance—Integrating terrestrial and aquatic
- carbon fluxes in a managed boreal forest landscape in Sweden. *Global Change Biology*,
- 685 26(4), 2353-2367. doi:https://doi.org/10.1111/gcb.14983

686	Christensen, T. R., Johansson, T., Olsrud, M., Strom, L., Lindroth, A., Mastepanov, M.,
687	Callaghan, T. V. (2007). A catchment-scale carbon and greenhouse gas budget of a
688	subarctic landscape. Philosophical Transactions of the Royal Society A: Mathematical,
689	Physical and Engineering Sciences, 365(1856), 1643-1656.
690	doi:10.1098/rsta.2007.2035
691	Clemmensen, K. E., Bahr, A., Ovaskainen, O., Dahlberg, A., Ekblad, A., Wallander, H.,
692	Lindahl, B. D. (2013). Roots and associated fungi drive long-term carbon sequestration
693	in boreal forest. Science, 339(6127), 1615-1618. doi:10.1126/science.1231923
694	Comyn-Platt, E., Hayman, G., Huntingford, C., Chadburn, S. E., Burke, E. J., Harper, A. B.,
695	. Sitch, S. (2018). Carbon budgets for 1.5 and 2 degrees C targets lowered by natural
696	wetland and permafrost feedbacks. Nature Geoscience, 11(8), 568-573.
697	doi:10.1038/s41561-018-0174-9
698	Delgado-Baquerizo, M., Oliverio, A. M., Brewer, T. E., Benavent-González, A., Eldridge, D.
699	J., Bardgett, R. D., Fierer, N. (2018). A global atlas of the dominant bacteria found
700	in soil. Science, 359(6373), 320. doi:10.1126/science.aap9516
701	Deng, J., McCalley, C. K., Frolking, S., Chanton, J., Crill, P., Varner, R., Li, C. S. (2017).
702	Adding stable carbon isotopes improves model representation of the role of microbial
703	communities in peatland methane cycling. Journal of Advances in Modeling Earth
704	Systems, 9(2), 1412-1430. doi:10.1002/2016ms000817
705	Etminan, M., Myhre, G., Highwood, E. J., & Shine, K. P. (2016). Radiative forcing of carbon
706	dioxide, methane, and nitrous oxide: A significant revision of the methane radiative
707	forcing. Geophysical Research Letters, 43(24), 12614-12623.
708	doi: https://doi.org/10.1002/2016GL071930
709	Frey, K. E., & Smith, L. C. (2007). How well do we know northern land cover? Comparison of
710	four global vegetation and wetland products with a new ground-truth database for West
711	Siberia. Global Biogeochemical Cycles, 21(1).
712	doi:https://doi.org/10.1029/2006GB002706

- 713 Friedlingstein, P., O'Sullivan, M., Jones, M. W., Andrew, R. M., Hauck, J., Olsen, A., . . .
- Zaehle, S. (2020). Global Carbon Budget 2020. Earth System Science Data, 12(4),
- 715 3269-3340. doi:10.5194/essd-12-3269-2020
- 716 Frieler, K., Lange, S., Piontek, F., Reyer, C. P. O., Schewe, J., Warszawski, L., . . . Yamagata,
- Y. (2017). Assessing the impacts of 1.5 degrees C global warming simulation protocol
- of the Inter-Sectoral Impact Model Intercomparison Project (ISIMIP2b). *Geoscientific*
- 719 *Model Development, 10*(12), 4321-4345. doi:10.5194/gmd-10-4321-2017
- Gauthier, S., Bernier, P., Kuuluvainen, T., Shvidenko, A. Z., & Schepaschenko, D. G. (2015).
- Boreal forest health and global change. Science, 349(6250), 819.
- 722 doi:10.1126/science.aaa9092
- 723 Gong, P., Liu, H., Zhang, M., Li, C., Wang, J., Huang, H., . . . Song, L. (2019). Stable
- classification with limited sample: transferring a 30-m resolution sample set collected
- in 2015 to mapping 10-m resolution global land cover in 2017. Science Bulletin, 64(6),
- 726 370-373. doi:<u>https://doi.org/10.1016/j.scib.2019.03.002</u>
- 727 Guo, M. Y., Zhuang, Q. L., Tan, Z. L., Shurpali, N., Juutinen, S., Kortelainen, P., &
- 728 Martikainen, P. J. (2020). Rising methane emissions from boreal lakes due to
- 729 increasing ice-free days. Environmental Research Letters, 15(6), 064008.
- 730 doi:10.1088/1748-9326/ab8254
- 731 Halabisky, M., Babcock, C., & Moskal, L. M. (2018). Harnessing the temporal dimension to
- improve object-based image analysis classification of wetlands. *Remote Sensing*, 10(9),
- 733 1467. doi:10.3390/rs10091467
- Heiskanen, L., Tuovinen, J. P., Räsänen, A., Virtanen, T., Juutinen, S., Lohila, A., . . . Aurela,
- 735 M. (2021). Carbon dioxide and methane exchange of a patterned subarctic fen during
- two contrasting growing seasons. *Biogeosciences*, 18(3), 873-896. doi:10.5194/bg-18-
- 737 873-2021
- Helbig, M., Chasmer, L. E., Kljun, N., Quinton, W. L., Treat, C. C., & Sonnentag, O. (2017).
- 739 The positive net radiative greenhouse gas forcing of increasing methane emissions

- from a thawing boreal forest-wetland landscape. Global Change Biology, 23(6), 2413-
- 741 2427. doi:10.1111/gcb.13520
- Helbig, M., Waddington, J. M., Alekseychik, P., Amiro, B. D., Aurela, M., Barr, A. G., . . .
- Zyrianov, V. (2020). Increasing contribution of peatlands to boreal evapotranspiration
- in a warming climate. Nature Climate Change, 555-560. doi:10.1038/s41558-020-
- 745 0763-7
- Hird, J. N., DeLancey, E. R., McDermid, G. J., & Kariyeva, J. (2017). Google Earth Engine,
- open-access satellite data, and machine learning in support of large-area probabilistic
- 748 wetland mapping. *Remote Sensing*, *9*(12). doi:10.3390/rs9121315
- Hopple, A. M., Wilson, R. M., Kolton, M., Zalman, C. A., Chanton, J. P., Kostka, J., . . .
- 750 Bridgham, S. D. (2020). Massive peatland carbon banks vulnerable to rising
- 751 temperatures. *Nature Communications*, 11(1). doi:10.1038/s41467-020-16311-8
- Hugelius, G., Loisel, J., Chadburn, S., Jackson, R. B., Jones, M., MacDonald, G., . . . Yu, Z.
- 753 (2020). Large stocks of peatland carbon and nitrogen are vulnerable to permafrost thaw.
- Proceedings of the National Academy of Sciences of the United States of America,
- 755 *117*(34), 20438-20446. doi:10.1073/pnas.1916387117
- Johansson, T., Malmer, N., Crill, P. M., Friborg, T., Akerman, J. H., Mastepanov, M., &
- 757 Christensen, T. R. (2006). Decadal vegetation changes in a northern peatland,
- greenhouse gas fluxes and net radiative forcing. Global Change Biology, 12(12), 2352-
- 759 2369. doi:10.1111/j.1365-2486.2006.01267.x
- Joos, F., Roth, R., Fuglestvedt, J. S., Peters, G. P., Enting, I. G., von Bloh, W., ... Weaver, A.
- J. (2013). Carbon dioxide and climate impulse response functions for the computation
- of greenhouse gas metrics: a multi-model analysis. Atmospheric Chemistry and
- 763 *Physics*, 13(5), 2793-2825. doi:10.5194/acp-13-2793-2013
- Juutinen, S., Valiranta, M., Kuutti, V., Laine, A. M., Virtanen, T., Seppa, H., . . . Tuittila, E. S.
- 765 (2013). Short-term and long-term carbon dynamics in a northern peatland-stream-lake
- 766 continuum: A catchment approach. Journal of Geophysical Research-Biogeosciences,
- 767 *118*(1), 171-183. doi:10.1002/jgrg.20028

- Karlson, M., Gålfalk, M., Crill, P., Bousquet, P., Saunois, M., & Bastviken, D. (2019).
- Delineating northern peatlands using Sentinel-1 time series and terrain indices from
- local and regional digital elevation models. Remote Sensing of Environment, 231,
- 771 111252. doi:https://doi.org/10.1016/j.rse.2019.111252
- Kicklighter, D. W., Melillo, J. M., Monier, E., Sokolov, A. P., & Zhuang, Q. L. (2019). Future
- nitrogen availability and its effect on carbon sequestration in Northern Eurasia. *Nature*
- 774 *Communications*, 10, 3024. doi:10.1038/s41467-019-10944-0
- Korpela, I., Haapanen, R., Korrensalo, A., Tuittila, E. S., & Vesala, T. (2020). Fine-resolution
- mapping of microforms of a boreal bog using aerial images and waveform-recording
- 777 LiDAR. Mires and Peat, 26. doi:10.19189/MaP.2018.OMB.388
- 778 Kou, D., Yang, G., Li, F., Feng, X., Zhang, D., Mao, C., . . . Yang, Y. (2020). Progressive
- 779 nitrogen limitation across the Tibetan alpine permafrost region. Nature
- 780 *Communications, 11*(1), 3331. doi:10.1038/s41467-020-17169-6
- 781 Krankina, O. N., Pflugmacher, D., Friedl, M., Cohen, W. B., Nelson, P., & Baccini, A. (2008).
- Meeting the challenge of mapping peatlands with remotely sensed data.
- 783 *Biogeosciences, 5*(6), 1809-1820. doi:10.5194/bg-5-1809-2008
- Laine, A., Riutta, T., Juutinen, S., Väliranta, M., & Tuittila, E. S. (2009). Acknowledging the
- spatial heterogeneity in modelling/reconstructing carbon dioxide exchange in a
- northern aapa mire. Ecological Modelling, 220(20), 2646-2655.
- 787 doi:https://doi.org/10.1016/j.ecolmodel.2009.06.047
- 788 Lawrence, D., Fisher, R., Koven, C., Oleson, K., Swenson, S., Vertenstein, M., . . . Xu, C.
- 789 (2018). *CLM5.0 Technical Description*. Boulder, CO: National Center for Atmospheric
- 790 Research.
- 791 Lehner, B., & Döll, P. (2004). Development and validation of a global database of lakes,
- reservoirs and wetlands. Journal of Hydrology, 296(1), 1-22.
- 793 doi:https://doi.org/10.1016/j.jhydrol.2004.03.028

- Li, C. S., Aber, J., Stange, F., Butterbach-Bahl, K., & Papen, H. (2000). A process-oriented
- model of N₂O and NO emissions from forest soils: 1. Model development. *Journal of*
- 796 Geophysical Research-Atmospheres, 105(D4), 4369-4384. doi:10.1029/1999jd900949
- 797 Li, T. T., Raivonen, M., Alekseychik, P., Aurela, M., Lohila, A., Zheng, X. H., . . . Zhang, W.
- 798 (2016). Importance of vegetation classes in modeling CH4 emissions from boreal and
- subarctic wetlands in Finland. Science of the Total Environment, 572, 1111-1122.
- doi:10.1016/j.scitotenv.2016.08.020
- 801 Lohila, A., Minkkinen, K., Laine, J., Savolainen, I., Tuovinen, J. P., Korhonen, L., . . .
- Laaksonen, A. (2010). Forestation of boreal peatlands: Impacts of changing albedo and
- greenhouse gas fluxes on radiative forcing. Journal of Geophysical Research-
- 804 *Biogeosciences, 115*, G04011. doi:10.1029/2010jg001327
- Loisel, J., Gallego-Sala, A. V., Amesbury, M. J., Magnan, G., Anshari, G., Beilman, D. W., . .
- 806 . Wu, J. (2021). Expert assessment of future vulnerability of the global peatland carbon
- sink. *Nature Climate Change*, 11(1), 70-77. doi:10.1038/s41558-020-00944-0
- Loveland, T. R., Reed, B. C., Brown, J. F., Ohlen, D. O., Zhu, Z., Yang, L., & Merchant, J. W.
- 809 (2000). Development of a global land cover characteristics database and IGBP
- 810 DISCover from 1 km AVHRR data. *International Journal of Remote Sensing*, 21(6-7),
- 811 1303-1330. doi:10.1080/014311600210191
- Lucht, W., Prentice, I. C., Myneni, R. B., Sitch, S., Friedlingstein, P., Cramer, W., . . . Smith,
- B. (2002). Climatic control of the high-latitude vegetation greening trend and Pinatubo
- effect. Science, 296(5573), 1687-1689. doi:10.1126/science.1071828
- Lund, M., Lafleur, P. M., Roulet, N. T., Lindroth, A., Christensen, T. R., Aurela, M., . . .
- Nilsson, M. B. (2010). Variability in exchange of CO₂ across 12 northern peatland and
- 817 tundra sites. Global Change Biology, 16(9), 2436-2448. doi:10.1111/j.1365-
- 818 2486.2009.02104.x
- 819 Mahdianpari, M., Salehi, B., Mohammadimanesh, F., Brisco, B., Homayouni, S., Gill, E., . . .
- 820 Bourgeau-Chavez, L. (2020). Big data for a big country: the first generation of
- Canadian wetland inventory map at a spatial resolution of 10-m using Sentinel-1 and

822	Sentinel-2 data on the Google Earth Engine cloud computing platform. Canadian
823	Journal of Remote Sensing, 46(1), 15-33. doi:10.1080/07038992.2019.1711366
824	Mathijssen, P. J. H., Kahkola, N., Tuovinen, J. P., Lohila, A., Minkkinen, K., Laurila, T., &
825	Valiranta, M. (2017). Lateral expansion and carbon exchange of a boreal peatland in
826	Finland resulting in 7000 years of positive radiative forcing. Journal of Geophysical
827	Research-Biogeosciences, 122(3), 562-577. doi:10.1002/2016jg003749
828	Matthews, E., Johnson, M. S., Genovese, V., Du, J., & Bastviken, D. (2020). Methane emission
829	from high latitude lakes: methane-centric lake classification and satellite-driven annual
830	cycle of emissions. Scientific Reports, 10(1), 12465. doi:10.1038/s41598-020-68246-1
831	Meinshausen, M., Smith, S. J., Calvin, K., Daniel, J. S., Kainuma, M. L. T., Lamarque, J. F.,
832	van Vuuren, D. P. P. (2011). The RCP greenhouse gas concentrations and their
833	extensions from 1765 to 2300. Climatic Change, 109(1), 213. doi:10.1007/s10584-
834	011-0156-z
835	Myhre, G., Shindell, D., Bréon, F. M., Collins, W., Fuglestvedt, J., Huang, J., Zhang, H.
836	(2013). Anthropogenic and Natural Radiative Forcing. In T. F. Stocker, D. Qin, GK.
837	Plattner, M. Tignor, S. K. Allen, J. Boschung, A. Nauels, Y. Xia, V. Bex, & P. M.
838	Midgley (Eds.), Climate Change 2013: The Physical Science Basis. Contribution of
839	Working Group I to the Fifth Assessment Report of the Intergovernmental Panel on
840	Climate Change. Cambridge, United Kingdom and New York, NY, USA: Cambridge
841	University Press.
842	Neubauer, S. C. (2021). Global warming potential is not an ecosystem property. <i>Ecosystems</i> .
843	doi:10.1007/s10021-021-00631-x
844	Nichols, J. E., & Peteet, D. M. (2019). Rapid expansion of northern peatlands and doubled
845	estimate of carbon storage. Nature Geoscience, 12(11), 917-921. doi:10.1038/s41561-
846	019-0454-z
847	O'Shea, S. J., Allen, G., Gallagher, M. W., Bower, K., Illingworth, S. M., Muller, J. B. A.,
848	Pyle, J. (2014). Methane and carbon dioxide fluxes and their regional scalability for the

849	European Arctic wetlands during the MAMM project in summer 2012. Atmospheric
850	
851	
852	D. (2021). The Boreal-Arctic Wetland and Lake Dataset (BAWLD). Earth System
853	Science Data Discussion, 2021, 1-40. doi:10.5194/essd-2021-140
854	Olson, D. M., Dinerstein, E., Wikramanayake, E. D., Burgess, N. D., Powell, G. V. N.,
855	Underwood, E. C., Kassem, K. R. (2001). Terrestrial Ecoregions of the World: A
856	New Map of Life on Earth: A new global map of terrestrial ecoregions provides an
857	innovative tool for conserving biodiversity. Bioscience, 51(11), 933-938.
858	doi:10.1641/0006-3568(2001)051[0933:TEOTWA]2.0.CO;2
859	Payette, S., Delwaide, A., Caccianiga, M., & Beauchemin, M. (2004). Accelerated thawing of
860	subarctic peatland permafrost over the last 50 years. Geophysical Research Letters,
861	31(18). doi: https://doi.org/10.1029/2004GL020358
862	Piilo, S. R., Korhola, A., Heiskanen, L., Tuovinen, JP., Aurela, M., Juutinen, S., Turunen,
863	J. (2020). Spatially varying peatland initiation, Holocene development, carbon
864	accumulation patterns and radiative forcing within a subarctic fen. Quaternary Science
865	Reviews, 248, 106596. doi: https://doi.org/10.1016/j.quascirev.2020.106596
866	Pirinen, P., Simola, H., Aalto, J., Kaukoranta, JP., Karlsson, P. S., & Ruuhela, R. (2012).
867	Climatological Statistics of Finland 1981-2010, Reports 2012:1. Helsinki, Finland:
868	Finnish Meteorological Institute.
869	Räsänen, A., Juutinen, S., Tuittila, E. S., Aurela, M., & Virtanen, T. (2019). Comparing ultra-
870	high spatial resolution remote-sensing methods in mapping peatland vegetation.
871	Journal of Vegetation Science, 30(5), 1016-1026. doi:10.1111/jvs.12769
872	Räsänen, A., Manninen, T., Korkiakoski, M., Lohila, A., & Virtanen, T. (2021). Predicting
873	catchment-scale methane fluxes with multi-source remote sensing. Landscape
874	Ecology, 36(4), 1177-1195. doi:10.1007/s10980-021-01194-x

- 875 Räsänen, A., & Virtanen, T. (2019). Data and resolution requirements in mapping vegetation
- in spatially heterogeneous landscapes. Remote Sensing of Environment, 230, 111207.
- 877 doi:10.1016/j.rse.2019.05.026
- 878 Sturtevant, C. S., & Oechel, W. C. (2013). Spatial variation in landscape-level CO₂ and CH₄
- fluxes from arctic coastal tundra: influence from vegetation, wetness, and the thaw lake
- 880 cycle. Global Change Biology, 19(9), 2853-2866. doi:10.1111/gcb.12247
- 881 Sulla-Menashe, D., Gray, J. M., Abercrombie, S. P., & Friedl, M. A. (2019). Hierarchical
- mapping of annual global land cover 2001 to present: The MODIS Collection 6 Land
- 883 Cover product. Remote Sensing of Environment, 222, 183-194.
- doi:https://doi.org/10.1016/j.rse.2018.12.013
- Tagesson, T., Schurgers, G., Horion, S., Ciais, P., Tian, F., Brandt, M., ... Fensholt, R. (2020).
- Recent divergence in the contributions of tropical and boreal forests to the terrestrial
- 887 carbon sink. *Nature Ecology & Evolution*, 4(2), 202-209. doi:10.1038/s41559-019-
- 888 1090-0
- Tan, Z., Zhuang, Q., & Anthony, K. W. (2015). Modeling methane emissions from arctic lakes:
- Model development and site-level study. Journal of Advances in Modeling Earth
- 891 *Systems*, 7(2), 459-483. doi:10.1002/2014ms000344
- Tan, Z., Zhuang, Q., Shurpali, N. J., Marushchak, M. E., Biasi, C., Eugster, W., & Anthony, K.
- W. (2017). Modeling CO₂ emissions from Arctic lakes: Model development and site-
- level study. Journal of Advances in Modeling Earth Systems, 9(5), 2190-2213.
- 895 doi:10.1002/2017ms001028
- Tang, J., Miller, P. A., Persson, A., Olefeldt, D., Pilesjo, P., Heliasz, M., . . . Christensen, T. R.
- 897 (2015). Carbon budget estimation of a subarctic catchment using a dynamic ecosystem
- model at high spatial resolution. *Biogeosciences*, 12(9), 2791-2808. doi:10.5194/bg-
- 899 12-2791-2015
- 900 Tanneberger, F., Tegetmeyer, C., Busse, S., Barthelmes, A., Shumka, S., Marine, A. M., . . .
- Joosten, H. (2017). The peatland map of Europe. Mires and Peat, 19.
- 902 doi:10.19189/MaP.2016.OMB.264

903	Thompson, D. K., Simpson, B. N., & Beaudoin, A. (2016). Using forest structure to predict the
904	distribution of treed boreal peatlands in Canada. Forest Ecology and Management, 372,
905	19-27. doi: https://doi.org/10.1016/j.foreco.2016.03.056
906	Treat, C. C., Marushchak, M. E., Voigt, C., Zhang, Y., Tan, Z., Zhuang, Q., Shurpali, N. J.
907	(2018). Tundra landscape heterogeneity, not interannual variability, controls the
908	decadal regional carbon balance in the Western Russian Arctic. Global Change
909	Biology, 24(11), 5188-5204. doi:10.1111/gcb.14421
910	Verpoorter, C., Kutser, T., Seekell, D. A., & Tranvik, L. J. (2014). A global inventory of lakes
911	based on high-resolution satellite imagery. Geophysical Research Letters, 41(18),
912	6396-6402. doi: <u>https://doi.org/10.1002/2014GL060641</u>
913	Weller, G., Chapin, F. S., Everett, K. R., Hobbie, J. E., Kane, D., Oechel, W. C., Walsh, J.
914	(1995). The arctic flux study: A regional view of trace gas release. Journal of
915	Biogeography, 22(2-3), 365-374. doi:10.2307/2845932
916	Xu, J. R., Morris, P. J., Liu, J. G., & Holden, J. (2018). PEATMAP: Refining estimates of
917	global peatland distribution based on a meta-analysis. Catena, 160, 134-140.
918	doi:10.1016/j.catena.2017.09.010
919	Zhang, Y., Chen, W. J., & Cihlar, J. (2003). A process-based model for quantifying the impact
920	of climate change on permafrost thermal regimes. Journal of Geophysical Research-
921	Atmospheres, 108(D22), 4695. doi:10.1029/2002jd003354
922	Zhang, Y., Sachs, T., Li, C., & Boike, J. (2012). Upscaling methane fluxes from closed
923	chambers to eddy covariance based on a permafrost biogeochemistry integrated model.
924	Global Change Biology, 18(4), 1428-1440. doi:10.1111/j.1365-2486.2011.02587.x

Acknowledgements

- 927 The authors acknowledge funding from Academy of Finland (CAPTURE Project
- 928 [#296423, #296887 and #296888]; Atmosphere and Climate Competence Center
- 929 (ACCC), 337550). The participant of C.C.T. was supported by ERC #851181 and the
- 930 Helmholtz Impulse and Networking Fund. J.D. was supported by NASA's
- 931 Interdisciplinary Research in Earth Science (Grant No. NNX17AK10G). N.C.
- 932 acknowledges funding from the FORMAS early career grant (contract no. 2019 -
- 933 01151).

934

935

926

Author contributions

- 936 D.K., T.V., C.C.T., J-P.T., N.J.S. and A.K. designed research and led the discussion,
- 937 A.R. and T.V. conducted the land cover classification, S.J., M.A., L.H. and J-P.T.
- performed the flux measurement, J.M., A.R. and T.V. conducted the soil and vegetation
- mapping, S.J., S.R.P., M.V., M.H., J.W. and T.J. collected data from peatland and water
- body properties, D.K., C.C.T., N.J.S., J.D., Y.Z., Q.Z. and M.G. performed the
- 941 biogeochemical modelling, J-P.T., D.K. and C.C.T. conducted the radiative forcing
- analysis, D.K., C.C.T. and J-P.T. analyzed data and integrated results, D.K., J-P.T.,
- 943 C.C.T., N.J.S. and A.K. drafted the manuscript. All authors contributed to the writing.

944

945

Competing interests

The authors declare that they have no competing interests.

947

948

ORCID

- 949 Dan Kou https://orcid.org/0000-0001-6116-9553
- 950 Claire Treat http://orcid.org/0000-0002-1225-8178

951	Juha-Pekka Tuovinen https://orcid.org/0000-0001-7857-036X
952	Aleksi Räsänen https://orcid.org/0000-0002-3629-1837
953	Narasinha J. Shurpali https://orcid.org/0000-0003-1052-4396
954	Christina Biasi https://orcid.org/0000-0002-7413-3354

Table 1. Land cover types (LCTs) and their dominant species in the tree, understory, and ground layers.

Land cover type Tree layer		Field layer	Ground layer		
Pine forest	Canopy cover > 10%, pine (<i>Pinus sylvestris</i>) cover > 2/3 of total canopy cover	Evergreen shrubs (e.g., Vaccinium vitis-idaea, Empetrum nigrum, and Calluna vulgaris), and also some deciduous shrubs	Feather mosses and lichens		
Birch forest	Canopy cover > 10%, birch (Betula pubescens) cover > 2/3 of total canopy cover	Evergreen and deciduous shrubs	Feather mosses and lichens		
Mixed forest	Multiple tree species, including pine, birch, and few aspen (<i>Populus tremula</i>), canopy cover > 10%, cover of minority species > 1/3	Evergreen (Vaccinium vitis-idaea) and deciduous (Vaccinium myrtillus, Vaccinium uliginosum) shrubs	Feather mosses and lichens		
Open forest	Forest with tree canopy cover < 10%	Evergreen shrubs, and some deciduous shrubs	Lichens, and some feather mosses		
Pine bog	Peatland with coverage of pine trees > 1%	Evergreen (<i>Rhododendron tomentosum</i>) and deciduous (<i>Vaccinium uliginosum, Betula nana</i>) shrubs, and some forbs (<i>Rubus chamaemorus</i>) and graminoids (mostly <i>Carex</i> spp.)	Sphagnum, feather mosses, and lichens		
Birch swamp	Peatland with coverage of birch trees > 2%	Forbs, grasses, and shrubs	Sphagnum and feather mosses		
String	Peatland with few trees (< 1% coverage)	Evergreen and deciduous dwarf shrubs as well as forbs (esp. <i>Rubus chamaemorus</i>)	Sphagnum and feather mosses, and some lichens		
Tall sedge fen	None	Sedges, also deciduous shrubs (e.g., Betula nana, Salix spp.) and forbs	Sphagnum, wet brown mosses, and open water		
Flark fen	None	Grasses and forbs	Open water, bare peat, and wet brown mosses		
Lake	None	None	Open water		
Stream	None	None	Open water		
Non-vegetated	None	None	Mostly human made bare areas, sand with some stones, and all roads in the area		

957 Table 2. The area extent of different land cover types (LCTs).

Major LCT	Specific LCT	Area (km²)	Area fraction (%)
Peatland	Pine bog	3.06	9.32
	Birch swamp	0.04	0.12
	String top	0.87	2.65
	String margin	0.60	1.83
	Tall sedge fen	1.85	5.64
	Flark fen	1.96	5.97
Forest	Pine forest	17.36	52.89
	Birch forest	0.14	0.43
	Mixed forest	1.94	5.91
	Open forest	0.44	1.34
Water body	Lake	4.32	13.16
	Stream	0.02	0.06
Non-vegetated		0.22	0.67
Total		32.82	100

Table 3. Assessment of peatland/wetland representation in different land cover products for the Kaamanen boreal landscape.

Product	Reference	Scale	Version	Methodology	Spatial resolution	Peatland/wetland relevant class label	Peatland/wetland area (%)	Spatial agreement (%)
Global Land Cover Characterization (GLCC)	Loveland et al. (2000)	Global	version 2	Remote sensing	1 km	-	0	0
Moderate Resolution Imaging Spectroradiometer Land Cover Type (MODIS.LCT)	Sulla-Menashe, Gray, Abercrombie, and Friedl (2019)	Global	MCD12Q1 v006	Remote sensing	500 m	-	0	0
Global Land Cover 2000 (GLC2000)	Bartholomé and Belward (2005)	Global	Global Product v1.1	Remote sensing	1 km	Regularly flooded shrub and/or herbaceous cover	58.0	21.8
Global Land Cover Map for 2009 (GlobCover2009)	Arino et al. (2012)	Global	v2.3	Remote sensing	300 m	Closed to open (>15%) grassland or woody vegetation on regularly flooded or waterlogged soil	0.1	0.1
First 10-m resolution global land cover product (FROM-GLC10)	Gong et al. (2019)	Global	v01	Remote sensing	10 m	Wetland	0.1	0.01
Global Lakes and Wetlands Database (GLWD)	Lehner and Döll (2004)	Global	level 3	Database	30 second	-	0	0
PEATMAP	Xu et al. (2018)	Global	Finland	Meta-analysis	Shapefile	Peatland	24.8	48.5
CORINE Land Cover 2018 EU, 25 ha (CLC2018EU.25ha)	https://land.copernicus.eu/pan- european/corine-land-cover/clc2018	Continental	2018, 25 ha	Remote sensing and database	Shapefile (minimum unit 25 ha)	Peatbog	25.3	44.8

CORINE Land Cover 2018 FI, 20	https://ckan.ymparisto.fi/dataset/corine-	National	2018, 20 m	Remote sensing and	20 m	BFPL, CFPL, MFPL, TWPL, peatbog, TIM,	28.6	62.0
m (CLC2018FI.20m)	maanpeite-2018	1 (40101141	2010, 20 111	database		and AIM		V=

Note: BFPL, CFPL, MFPL, TWPL, TIM, and AIM indicate *Broad-leaved forest on peatland, Coniferous forest on peatland, Mixed forest on peatland, Transitional woodland/shrub cc 10-30% on peatland* (cc = canopy closure), *Terrestrial inland marsh*, and *Aquatic inland marsh*, respectively.

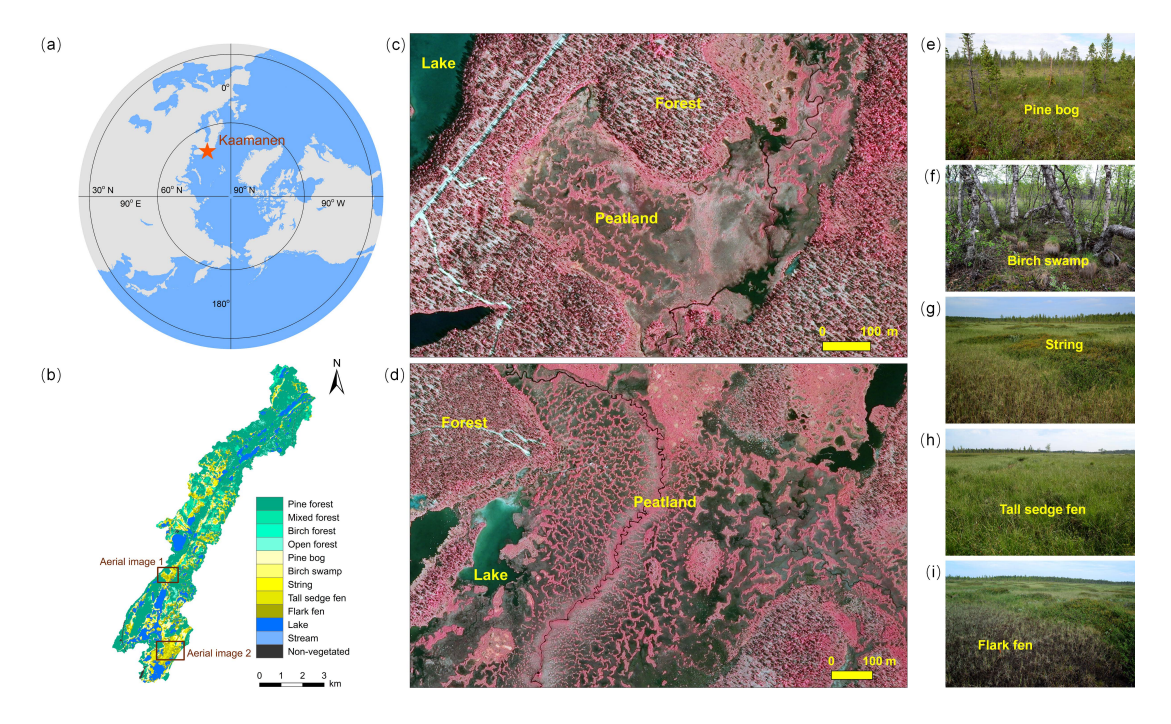


Figure 1. Location (a), land cover types (b), 0.5-m resolution false color aerial images (c-d), and photographs of different peatland types (e-i) of the Kaamanen catchment. Panels (c) and (d) correspond to Areal image 1 and 2, respectively, in panel (b).

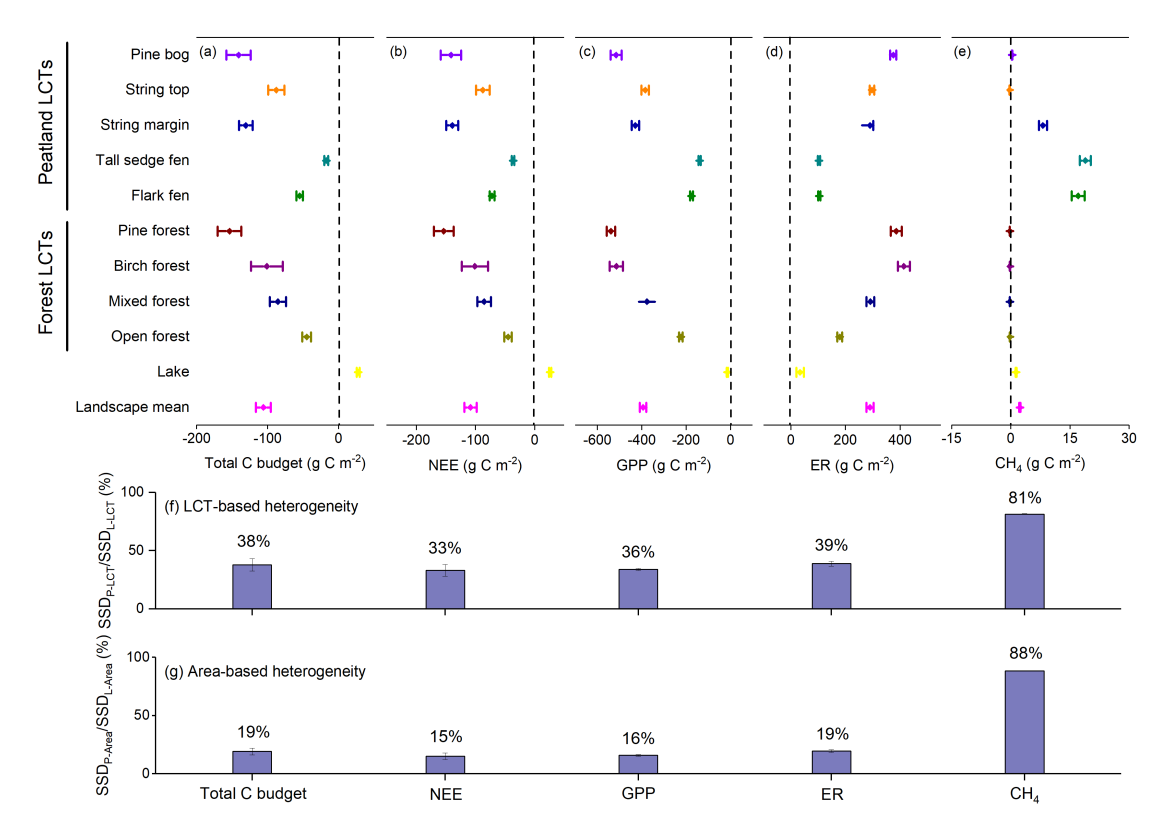


Figure 2. Heterogeneity in carbon (C) budget within the Kaamanen boreal landscape during 2005-2018. (a) Net C budgets combining carbon dioxide (CO₂) and methane (CH₄) among land cover types (LCTs) and their area-weighted landscape mean; (b) CO₂ budgets (net ecosystem CO₂ exchange, NEE); (c) Gross primary productivity (GPP); (d) Ecosystem respiration (ER); (e) CH₄ budgets; (f) Ratio between the Sum of Squared Deviations (SSD) from the arithmetic mean C budget among peatland LCTs (SSD_{P-LCT}) and that among all landscape LCTs (SSD_{L-LCT}); (g) Ratio between the SSD from the area-weighted landscape mean among peatland LCTs (SSD_{P-Area}) and that among all landscape LCTs (SSD_{L-Area}). In panels (a)-(e), a positive value means output from the ecosystem being a C output. The diamond symbol in panels (a)-(e) and the bar and number in panels (f)-(g) indicate the mean annual value, and the error bar in all panels denotes the 95% confidence interval.

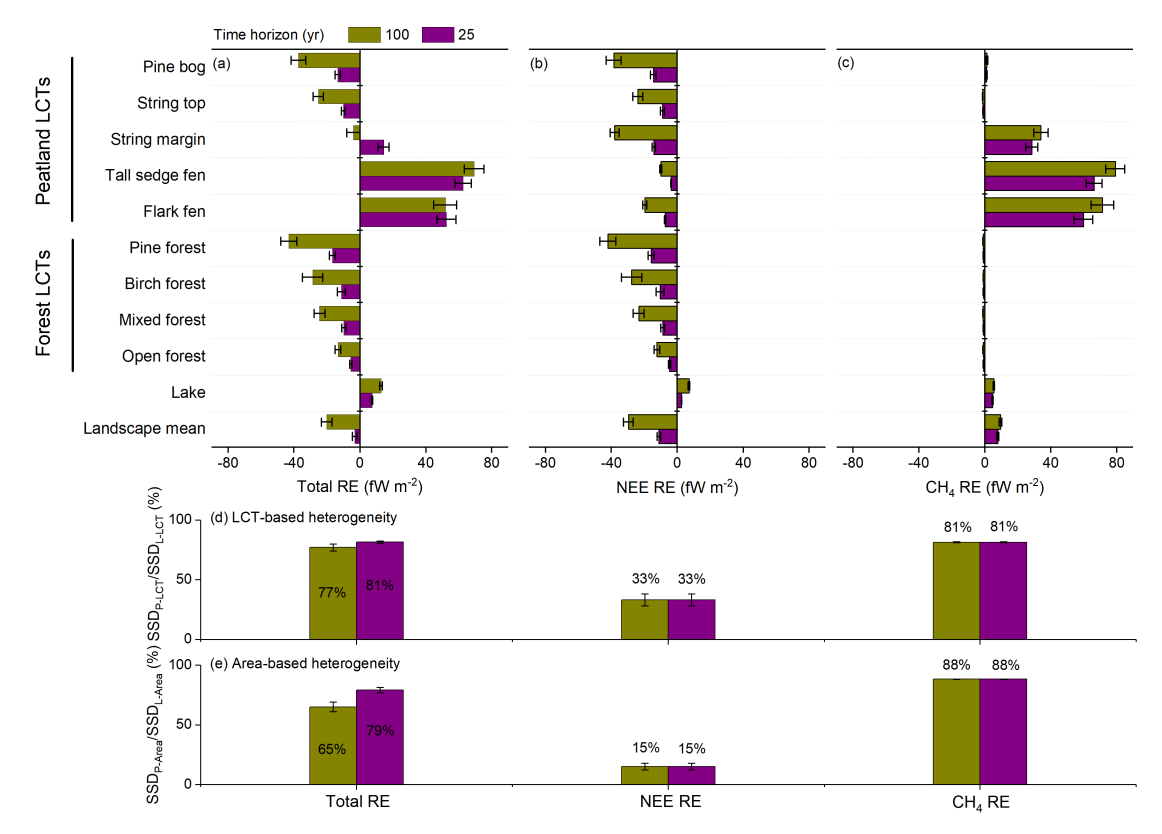


Figure 3. Heterogeneity in radiative effect (RE) of present carbon (C) budget within the Kaamanen boreal landscape. (a) Total RE due to carbon dioxide (CO₂) and methane (CH₄) exchange of different land cover types (LCTs) and their area-weighted landscape mean; (b) RE due to CO₂ exchange; (c) RE due to CH₄ exchange; (d) Ratio between the Sum of Squared Deviations (SSD) from the arithmetic mean RE among peatland LCTs (SSD_{P-LCT}) and that among all landscape LCTs (SSD_{L-LCT}); (e) Ratio between the SSD from the area-weighted landscape mean among peatland LCTs (SSD_{P-Area}) and that among all landscape LCTs (SSD_{L-Area}). The RE represents the cumulative RE due to an annual emission or uptake pulse over time horizons of 25 and 100 yr, calculated based on C flux densities (g m⁻² yr⁻¹, i.e., flux per m² of each LCT) during 2005-2018 and assuming the RCP4.5 scenario. The diamond symbol in panels (a)-(c) and the bar and number in panels (d)-(e) indicate the mean annual value, and the error bar in all panels denotes the 95% confidence interval. 1fW = 10⁻¹⁵ W.

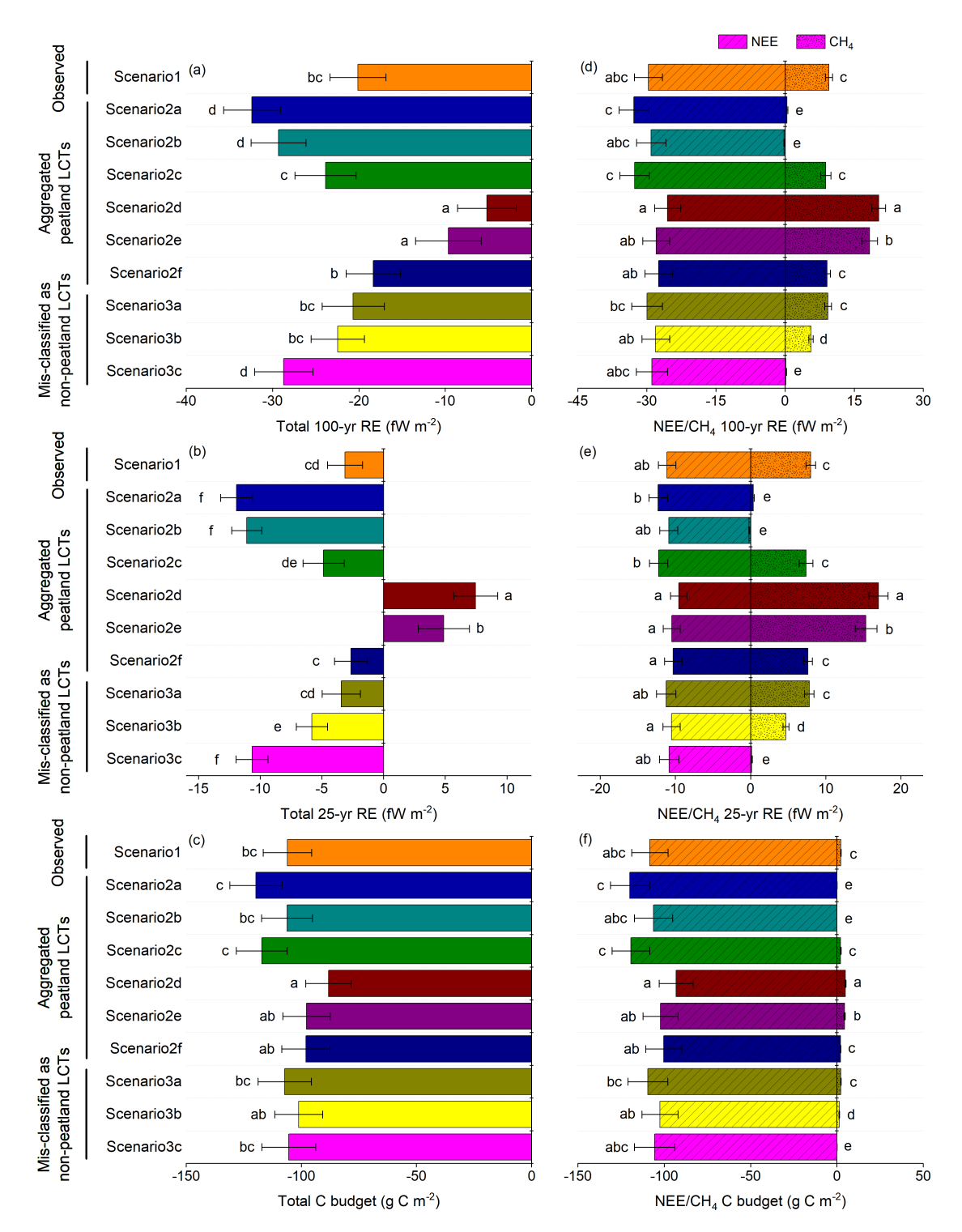


Figure 4. Uncertainty in radiative effect (RE) of landscape-scale carbon (C) budget due to aggregation or misclassification of peatlands. RE is calculated based on the C budget during 2005-2018 assuming the RCP4.5 scenario. (a-b) Total RE calculated based on landscape-scale total C budget with 100-yr and 25-yr time horizons; (c) Landscape-scale total C budget during 2005-2018; (d-e) RE calculated based on

landscape-scale CO₂ and CH₄ budgets with 100-yr and 25-yr time horizons; (f) Landscape-scale CO₂ and CH₄ budgets. RCP4.5 scenario is assumed for RE. Scenario 1 is based on the observed land cover type (LCT) data described in Table 2. In scenario 2, peatlands are not distinguished but assumed to consist of a single type (in 2a-2e, pine bog, string top, string margin, tall sedge fen, and flark fen, respectively). In scenario 2f, all dry peatlands are allocated to string top and all water-logged peatlands are classified as tall sedge fen. In scenario 3, peatlands are mis-classified as non-peatland LCTs: (3a) forested peatlands (pine bog and birch swamp) as corresponding forests (pine and birch forest, respectively), (3b) the open water-logged peatland with low vegetation cover (flark fen) as lake, and (3c) the simultaneous occurrence of scenarios 3a and 3b and a misclassification of all other open peatlands (string top, string margin, and tall sedge fen) as open dry peatland (represented by string top). The bar and error bar in the plot represent the mean value and its 95% confidence interval, respectively, and the letters denote the statistical difference among different scenarios. 1fW = 10⁻¹⁵ W.

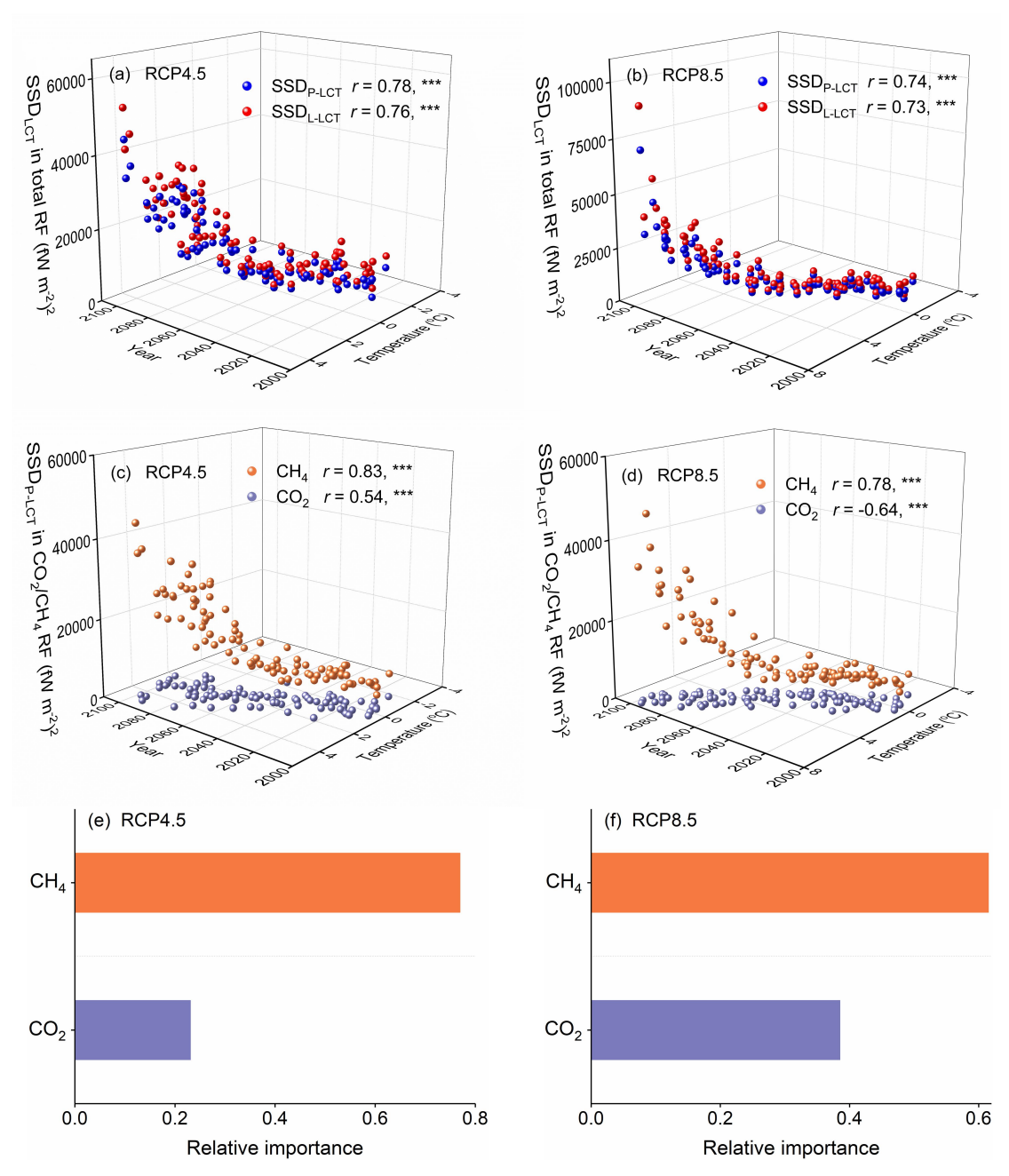


Figure 5. Potential trajectory of heterogeneity in radiative effect (RE) among different land cover types (LCTs) under future warming scenarios (RCP4.5 and RCP8.5). RE represents the cumulative RE due to an annual emission or uptake pulse over the 100-yr time horizon, calculated based on flux densities (g m⁻² yr⁻¹, i.e., flux per m² of each LCT) of CO₂ and methane CH₄ during 2005-2099. (a)-(b) Sum of Squared Deviations (SSD) from the mean total RE among peatland LCTs (SSD_{P-LCT}) and that among all landscape LCTs (SSD_{L-LCT}); (c)-(d) SSD_{P-LCT} of the CO₂- and CH₄-induced

RE; (e)-(f) Relative importance of CO₂ and CH₄ in explaining the trend in total RE heterogeneity among peatlands. *** denotes p < 0.001. In all panels, r denotes the correlation coefficient between SSD and temperature. To reflect warming effects, biogeochemical models were driven with variable temperature while other input data were kept constant (2005-2018 averages). 1fW = 10^{-15} W.

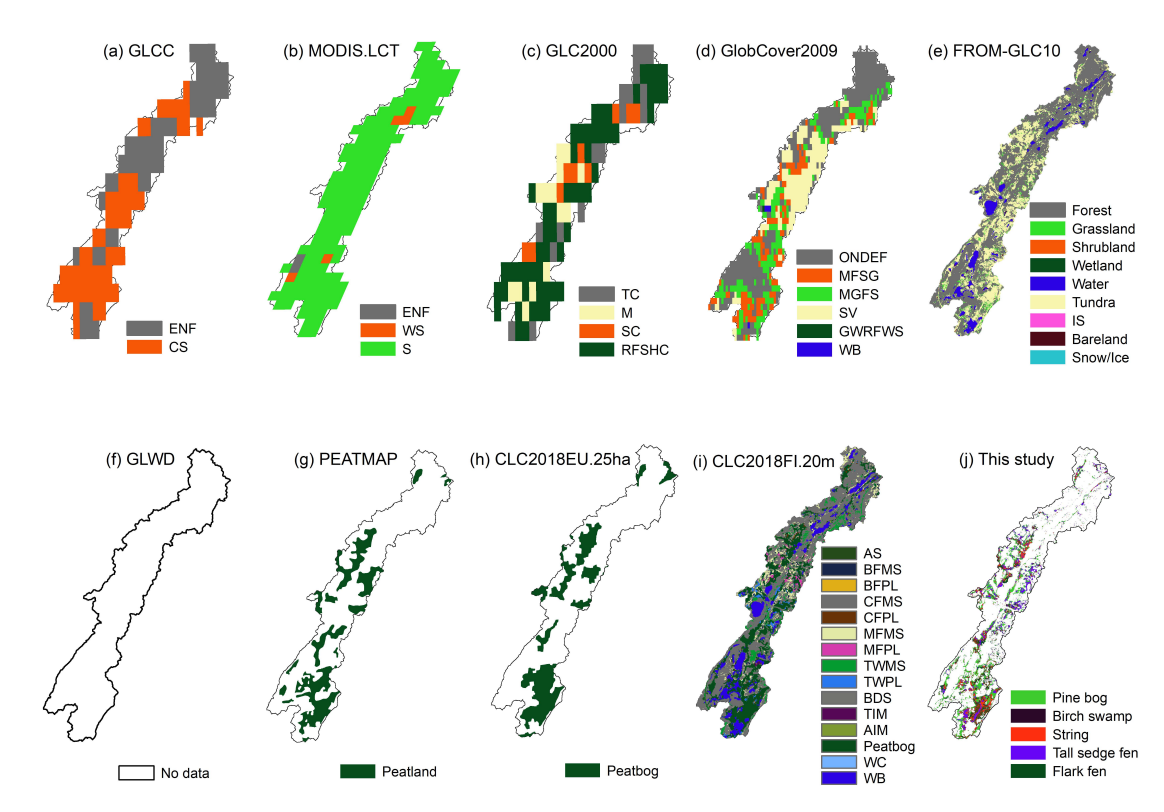


Figure 6. Land cover of the Kaamanen boreal landscape classified by global (a-g), continental (h), and national (i) land cover products and this study (j). (a) GLCC; (b) MODIS.LCT; (c) GLC2000; (d) GlobCover2009; (e) FROM-GLC10; (f) GLWD; (g) PEATMAP; (h) CLC2018EU.25ha; (i) CLC2018FI.20m; (j) Peatland types revealed by this study. For GLCC, ENF = Evergreen Needleleaf Forest and CS = Closed Shrublands, respectively; for MODIS.LCT, ENF = Evergreen Needleleaf Forests, WS = Woody Savannas, and S = Savannas, respectively; for GLC2000, TC = Tree Cover (needle-leaved, evergreen), M = Mosaic (Tree cover / Other natural vegetation), SC = Shrub Cover (closed-open, deciduous (with or without sparse tree layer)), and RFSHC = Regularly flooded shrub and/or herbaceous cover, respectively; for GlobCover2009, ONDEF = Open (15-40%) needleleaved deciduous or evergreen forest (>5m), MFSG = Mosaic forest or shrubland (50-70%) / grassland (20-50%), MGFS = Mosaic grassland (50-70%) / forest or shrubland (20-50%), SV = Sparse (<15%) vegetation, GWRFWS = Closed to open (>15%) grassland or woody

1043 vegetation on regularly flooded or waterlogged soil - Fresh, brackish or saline water, and WB = Water bodies, respectively; for FROM-GLC10, IS = Impervious surface; for 1044 CLC2018EU.25ha, there are three classes within the Kaamanen landscape (Coniferous 1045 1046 forest, Peatbog, Water body) and only Peatbog is shown here; for CLC2018FI.20m, AS = Artificial surface, BFMS = Broad-leaved forest on mineral soil, BFPL = Broad-1047 leaved forest on peatland, CFMS = Coniferous forest on mineral soil, CFPL = 1048 Coniferous forest on peatland, MFMS = Mixed forest on mineral soil, MFPL = Mixed 1049 forest on peatland, TWMS = Transitional woodland/shrub on mineral soil, TWPL = 1050 1051 *Transitional woodland/shrub on peatland*, BDS = Beach, dune, and sand plain, TIM = Terrestrial inland marsh, AIM = Aquatic inland marsh, WC = Water course, and WB 1052 1053 = Water body, respectively; for our classification, only peatland classes are shown here. 1054 More information about the land cover products is presented in Table 3.